actuators

MDPI

Article

Fault-Tolerant Redesign of a Quad-Winding PMSM to Prevent Irreversible Partial Demagnetization

Min-Seong Jo [1], Young-Joon Song [1], Kyung-il Woo [2,*] and Kyu-Yun Hwang [1,3,*]

[1] School of Electronic Engineering, Kumoh National Institute of Technology, Gumi 39177, Republic of Korea; dufhfhdu@naver.com (M.-S.J.); yjsong@kumoh.ac.kr (Y.-J.S.)
[2] Department of Electrical Engineering, Pukyong National University, Busan 48513, Republic of Korea
[3] Department of IT Convergence Engineering, Kumoh National Institute of Technology, Gumi 39177, Republic of Korea
* Correspondence: cogging@pknu.ac.kr (K.-i.W.); kyhwang@kumoh.ac.kr (K.-Y.H.)

Abstract

This paper proposes a fault-tolerant optimal design method for quad-winding permanent magnet synchronous motors (PMSMs) considering irreversible demagnetization under fault conditions. In quad-winding motors, when one or more winding sets become unavailable, the remaining windings must carry higher current to maintain the required torque. This increases the external magnetomotive force acting on the permanent magnets and may cause irreversible demagnetization, particularly in spoke-type magnet structures. To address this issue, the demagnetization characteristics of the quad-winding motor were analyzed under healthy and faulty operating conditions. Based on this analysis, an optimization process using a Radial Basis Function–Multi-Layer Perceptron (RBF–MLP) surrogate model and a combination of grid-based search and local optimization was applied to obtain an optimal motor design. The optimization results show that the irreversible demagnetization ratio was reduced from 5.9% to 0.5% while maintaining a similar magnet volume. The proposed design approach effectively suppresses irreversible demagnetization in quad-winding PMSMs.

Keywords: brushless AC motor; spoke type interior permanent magnet motor; irreversible demagnetization; demagnetization rate; RBF-MLP surrogate model; fault-tolerant; quad-winding

1. Introduction

Permanent magnet synchronous motors (PMSMs) are widely used in high-performance applications such as electric vehicles (EVs), aerospace systems, and robotic actuators due to their high efficiency, high power density, and compact structure [1]. As the reliability requirements of these applications continue to increase, ensuring safe and stable operation of motor drive systems under fault conditions has become a critical issue. In practical operating environments, motors may experience faults such as open-circuit faults, short-circuit faults, and inverter failures. These faults can lead to severe torque ripple, performance degradation, or even complete system shutdown. Accordingly, fault-tolerant motor systems capable of maintaining operation under faulty conditions have been extensively studied.

Many studies have focused on fault-tolerant control strategies that allow motors to continue operating after faults occur. Control techniques such as model predictive control and reconfigurable control methods have been proposed to improve drive system reliability [2–4]. In addition to control-based approaches, system-level redundancy using

Check for updates

Academic Editor: Dong Jiang

Received: 16 March 2026
Revised: 23 April 2026
Accepted: 29 April 2026
Published: 30 April 2026

Copyright: © 2026 by the authors. Licensee MDPI, Basel, Switzerland. This article is an open access article distributed under the terms and conditions of the Creative Commons Attribution (CC BY) license.

multiple motors has also been investigated. For example, redundant motor systems have been applied to electric power steering systems and electric vehicle traction systems to enhance operational reliability [5,6]. However, these approaches generally increase system complexity, cost, and volume because additional motors, inverters, and control systems are required.

To improve reliability without system complexity, fault-tolerant motor topologies based on multi-winding configurations have been widely studied. Among them, dual-winding permanent magnet machines have attracted considerable attention because they can maintain continuous operation even when one winding set becomes faulty. Dual-winding PMSMs have been investigated for high-reliability applications including aerospace drive systems and fault-tolerant motor drives [7–9]. In addition, several studies have analyzed the fault characteristics of dual-winding machines depending on the winding arrangement and phase configuration [10].

Although dual-winding machines can provide fault-tolerant capability, their redundancy is still limited because only one additional winding set is available. To further enhance reliability, multi-redundant motor structures employing more than two winding sets have been investigated [11]. In particular, quad-winding PMSMs provide higher redundancy than dual-winding machines because the load torque can still be maintained even when multiple winding sets fail by redistributing the load among the remaining windings. Therefore, quad-winding configurations have emerged as a promising solution for high-reliability motor drive systems.

However, a key issue problem arises in quad-winding PMSMs under winding-fault conditions. When one or more winding sets fail, the remaining windings must carry increased currents in order to maintain the required load torque. In severe cases such as triple-winding faults, the current flowing in the remaining winding may increase several times compared with the rated current. This excessive current produces strong demagnetizing magnetic fields inside the permanent magnets and may lead to irreversible demagnetization. Irreversible demagnetization is one of the major failure mechanisms in permanent magnet machines because it permanently degrades motor performance and cannot be recovered once it occurs [12,13].

To mitigate this problem, several studies have investigated motor design methods considering irreversible demagnetization during the design stage. For example, optimal design approaches considering partial demagnetization have been proposed for spoke-type interior permanent magnet motors, where irreversible demagnetization can cause magnetic flux imbalance and increase torque ripple and cogging torque [14,15]. In addition, hybrid magnet structures combining NdFeB and ferrite magnets have been investigated to improve demagnetization resistance and overall motor reliability [16]. Various optimization-based motor design approaches have also been explored to improve electromagnetic performance and reliability, including optimal rotor design methods and system-level motor optimization techniques [17–19].

Despite these research efforts, most existing studies have focused on demagnetization under normal operating conditions or specific motor structures. The demagnetization problem caused by current redistribution under winding-fault conditions in quad-winding PMSMs has not been sufficiently investigated. In quad-winding machines, the redistribution of current under one to three winding faults can extensively increase the demagnetization risk because the remaining windings must carry much higher currents to maintain the same load torque [20]. Therefore, it is necessary to develop a motor design methodology that simultaneously considers the fault-tolerant characteristics of quad-winding PMSMs and the irreversible demagnetization problem caused by current increase under fault conditions.

In this paper, a fault-tolerant optimal design method for quad-winding PMSMs considering irreversible demagnetization under fault conditions is presented. Under winding fault conditions, current redistribution among the remaining windings increases the external magnetomotive force acting on the permanent magnets, which may lead to irreversible demagnetization. To address this issue, an optimization framework based on a Radial Basis Function–Multi-Layer Perceptron (RBF–MLP) surrogate model and a combination of grid-based search and local optimization is applied to obtain a motor design that suppresses irreversible demagnetization while maintaining magnet volume.

The main contributions of the paper can be summarized as follows:

(1) The irreversible demagnetization mechanism in quad-winding PMSMs is analyzed under winding fault conditions, explicitly considering the effect of current redistribution among the remaining windings.
(2) A design framework is proposed to address the coupled relationship between fault-induced current increase and irreversible demagnetization, which is not considered in conventional motor design approaches.
(3) A surrogate-model-based optimization process is developed to mitigate irreversible demagnetization while preserving motor performance under fault conditions.
(4) The effectiveness of the proposed method is demonstrated by reducing the irreversible demagnetization ratio from 5.9% to 0.5% while maintaining a comparable magnet volume.

The remainder of this paper is organized as follows. Section 2 describes the quad-winding motor configuration and its fault-tolerant characteristics. Section 3 presents the multi-objective optimization process considering irreversible demagnetization. Finally, Section 4 concludes the paper.

2. Quad-Winding Motor Configuration and Fault-Tolerant Characteristics

2.1. Configuration of Quad-Winding Motor

Figure 1 shows the conceptual configuration of the proposed quad-winding motor control system. The overall system consists of a quad electronic control unit (Quad-ECU), four independent current control loops, four inverters, and a quad-winding PMSM. Each winding set is controlled independently while sharing the same speed command. The control structure includes a speed controller, an MTPA and flux-weakening block, and a current reference generation unit. Based on the ECU fault signal, the controller operates either in a normal steady-state mode or in a fault-tolerant mode. In the event of a winding fault, the system redistributes the current command among the remaining healthy windings, allowing continuous motor operation.

Figure 2 illustrates the physical configuration of the quad-winding motor and the corresponding circuit connection. The stator contains four electrically isolated three-phase winding sets, each of which is connected to an independent inverter. These winding sets are spatially distributed in the stator slots to reduce electromagnetic coupling and improve fault isolation capability. The rotor consists of permanent magnets embedded in the rotor core, while the stator core accommodates the distributed winding structure. Because each winding group operates independently, the motor can maintain torque production even when one or more winding sets are unavailable. The independent winding configuration provides inherent fault-tolerant capability. When a fault occurs in a specific winding set, the corresponding inverter can be isolated from the system without interrupting the operation of the remaining windings. As a result, the proposed quad-winding configuration improves system reliability compared with conventional single-winding or dual-winding motor structures.

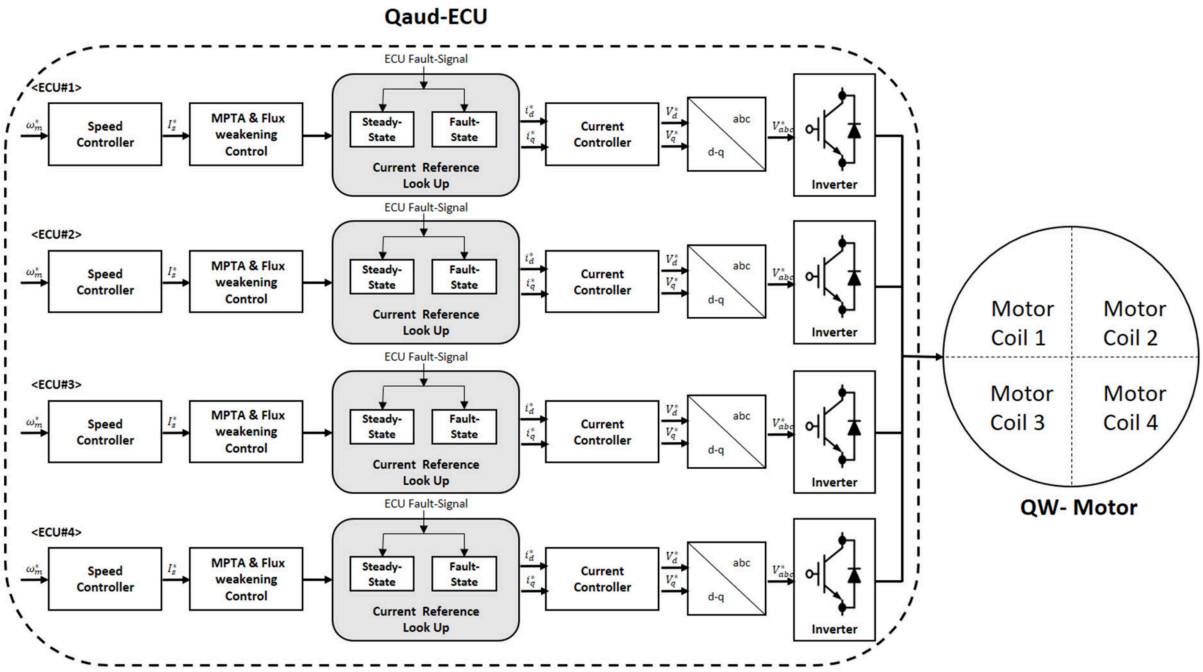


Figure 1. Conceptual Diagram of Quad-Winding Control System.

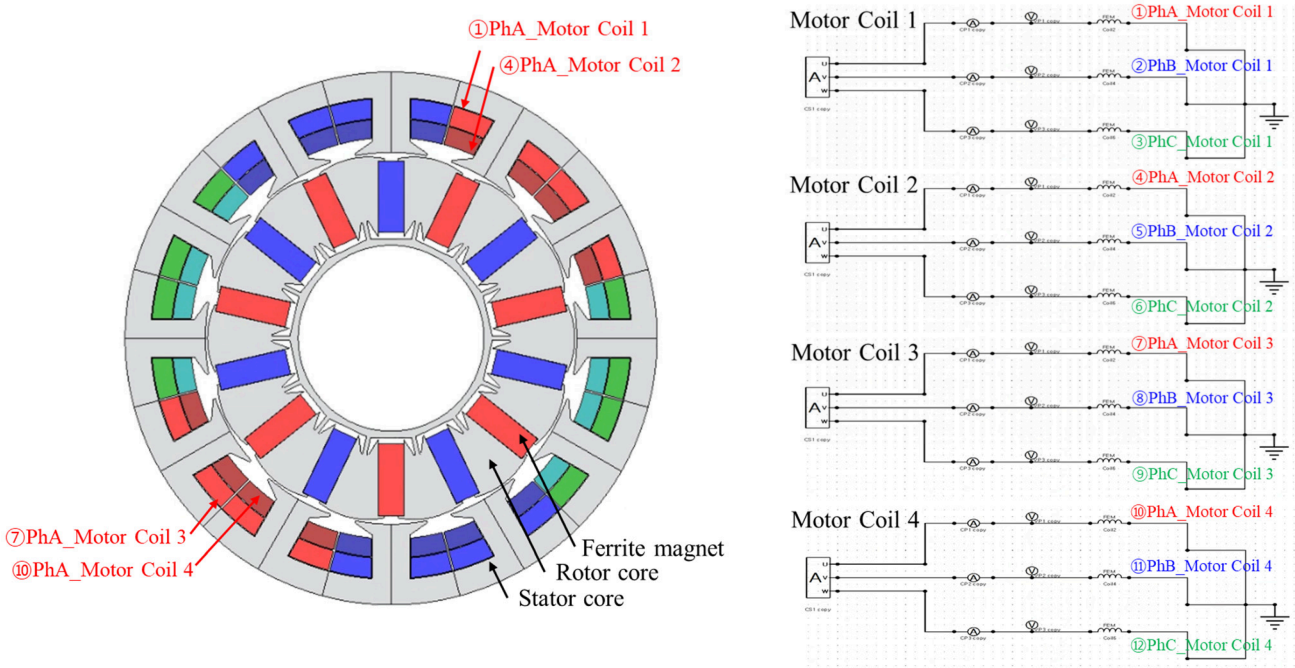


Figure 2. Quad-winding motor and circuit diagram.

Table 1 summarizes the main specifications of the motor used in this study. The motor is designed for a mobile robot drive system and has a rated torque of 5 Nm and a rated current of 50 Apk. The stator outer diameter is 126 mm and the air-gap length is 0.5 mm. The stator core is made of 50PN470 electrical steel. These specifications were selected to provide sufficient torque capability while maintaining a compact motor structure suitable for mobile robotic applications.

Table 1. Main design parameters of the Drive Motor for a Mobile Robot.

Items	Unit	Value	Items	Unit	Value
Stator outer diameter	mm	126	Magnet length	mm	17
Stator inner diameter	mm	88	Magnet thickness	mm	6
Air-gap length	mm	0.5	Tooth width	mm	9
Rotor outer diameter	mm	87	Yoke thickness	mm	6
Pole pair number	-	7	Core material	-	50PN470
Number of slots	-	12	Rated Torque	Nm	5
Number of turns per slot	-	10	Rated Current	Apk	50

The rated current and target torque were determined considering a low-voltage battery-driven application, where a torque level of approximately 5 Nm is within a practical range. The current rating and inverter capacity were selected considering fault-tolerant operation of the quad-winding motor. Therefore, a maximum current of 120 Apk was considered, providing sufficient margin for fault conditions and thermal constraints.

2.2. Motor Characteristics Under Healthy and Faulty Modes

The motor characteristics under healthy and faulty operating conditions were analyzed to evaluate the fault-tolerant capability of the proposed quad-winding motor. Figure 3 shows the torque and current characteristics of the quad-winding motor under healthy and faulty operating conditions.

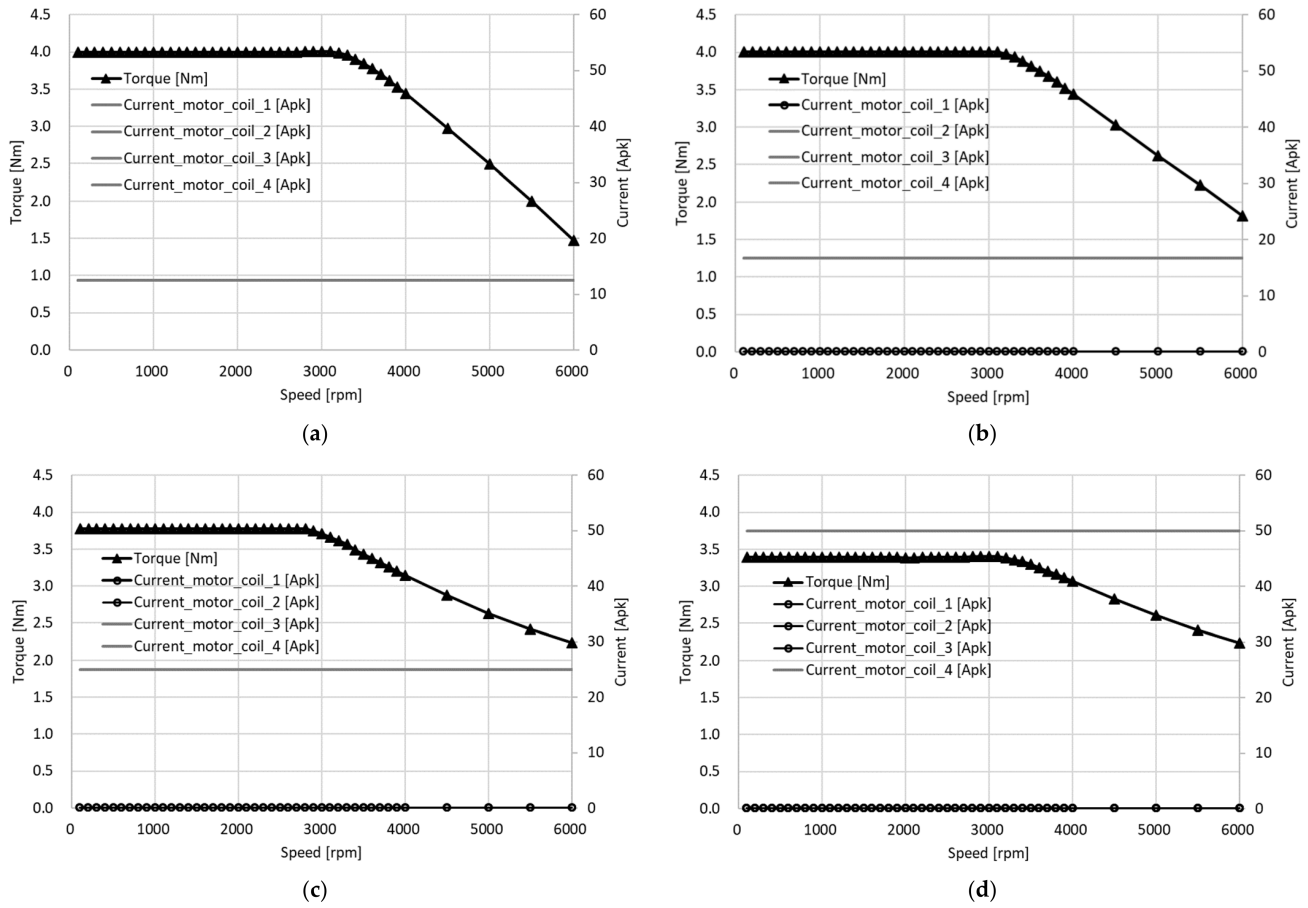


Figure 3. Torque and current characteristics of the quad-winding motor under healthy and faulty operating conditions: (**a**) healthy condition, (**b**) one winding faulty, (**c**) two windings faulty, and (**d**) three windings faulty.

In the healthy condition shown in Figure 3a, all four motor coils operate normally and the torque is evenly shared by the four winding sets. As a result, each coil carries the same current over the operating speed range. Figure 3b represents the case where motor coil 1 is faulty due to an ECU fault. To maintain the same torque output, the remaining motor coils 2, 3, and 4 compensate for the loss of one winding. Consequently, the current of the active windings increases to approximately 4/3 of the normal condition.

As shown in Figure 3, the required current increases as the number of available windings decreases under fault conditions. The increase in current produces a stronger demagnetizing magnetic field acting on the permanent magnets. To evaluate this effect, irreversible demagnetization was analyzed for each operating condition by applying the maximum current corresponding to each fault case. Figure 4 presents the irreversible demagnetization distribution in the permanent magnet under these operating conditions. Irreversible demagnetization appears near the upper region of the magnet when the maximum current is applied. In spoke-type permanent magnet motors, the upper part of the magnet is strongly influenced by the external magnetomotive force (MMF), making this region particularly susceptible to irreversible demagnetization [14]. The demagnetization distributions in Figure 4a,b are nearly identical because the magnitude of the external MMF generated by the winding configuration is the same in both cases. A similar tendency is also observed in Figure 4c,d, where the resulting external MMF acting on the magnet becomes identical.

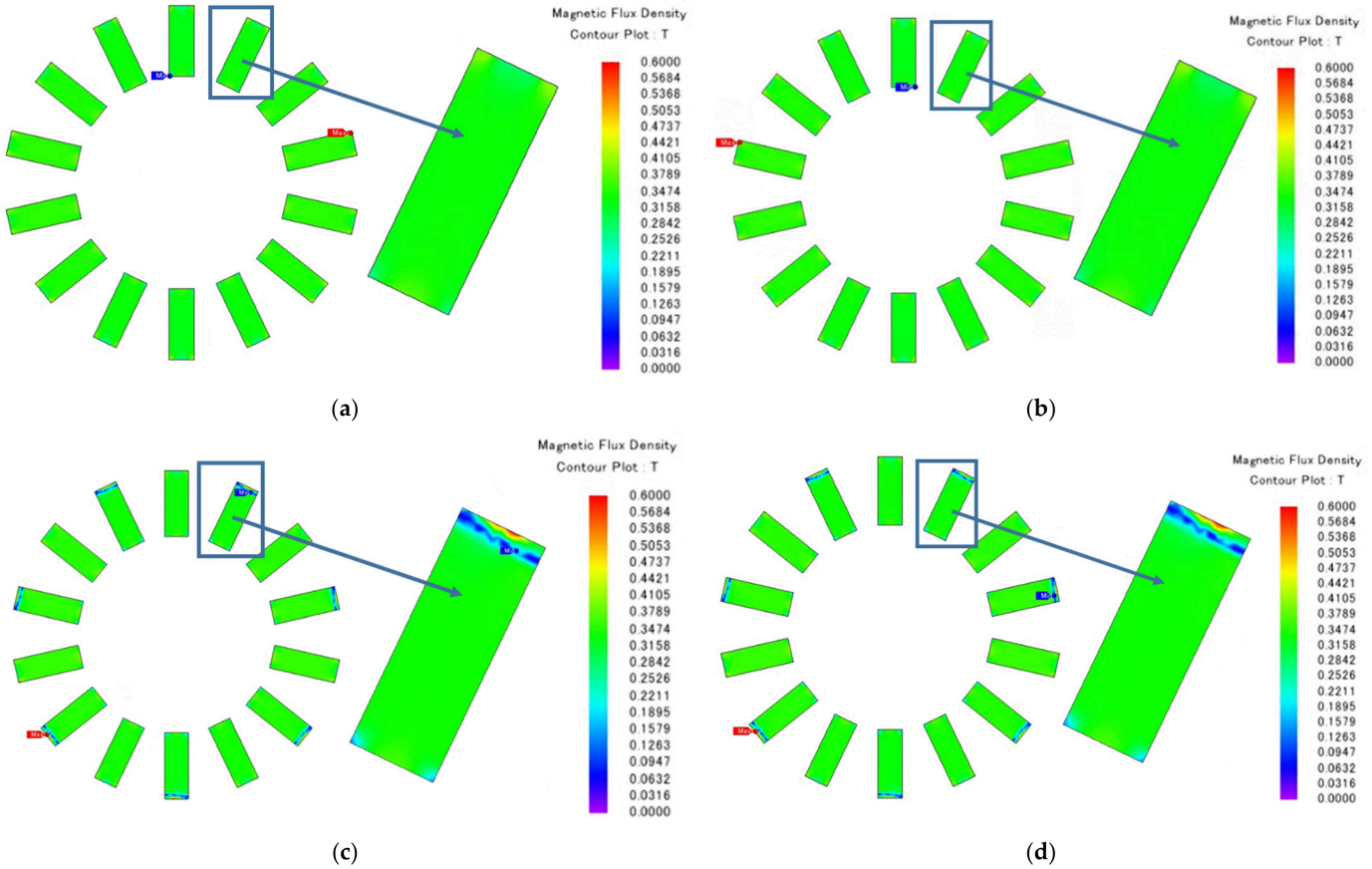


Figure 4. Irreversible demagnetization distribution in the spoke-type permanent magnet under maximum current conditions: (**a**) healthy condition, (**b**) one winding fault, (**c**) two winding faults, and (**d**) three winding faults.

These results illustrate that dividing a conventional motor into multiple winding groups to form a quad-winding motor can lead to an increase in current under fault con-

ditions. The resulting demagnetizing field may cause irreversible demagnetization of the permanent magnets, which can degrade the electromagnetic performance of the motor. Therefore, an appropriate motor design is required to minimize irreversible demagnetization when the motor is operated as a quad-winding configuration.

3. Multi-Objective Optimization of Quad-Winding PMSM

This section describes the multi-objective optimization process for the quad-winding PMSM. The objective of the proposed optimization is to reduce irreversible demagnetization under winding fault conditions while minimizing magnet usage. To achieve this goal, a surrogate-model-based optimization process is employed. The overall optimization procedure consists of five steps, including the selection of design variables, generation of initial samples using Latin Hypercube Sampling (LHS), FEM analysis, surrogate model construction using an RBF–MLP, and optimal design search. The optimization process is illustrated in Figure 5. In the optimization stage, a combination of grid-based search and local optimization using the Nelder–Mead method is employed to identify the optimal design.

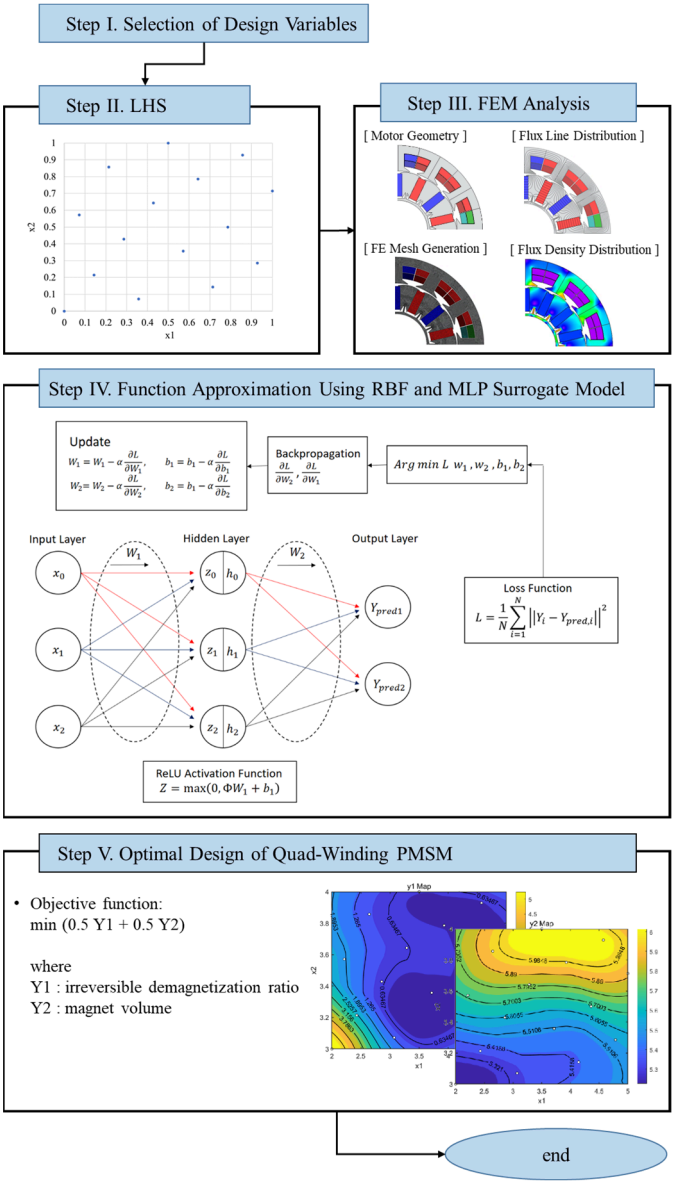


Figure 5. Quad-Winding PMSM Optimization Process.

3.1. Selection of Design Variables (Step I)

In the proposed optimization process, the geometric parameters that affect the irreversible demagnetization characteristics of the motor are selected as design variables. As shown in Figure 6, the magnet width and magnet stack length are chosen as the primary design variables. In this study, the optimization focuses on key design parameters that strongly influence irreversible demagnetization in spoke-type PMSMs, particularly the magnet width and magnet stack length selected in the paper. Compared to other geometric parameters such as air-gap dimensions or tooth and pole shapes, these parameters have a more direct impact on demagnetization behavior under fault conditions.

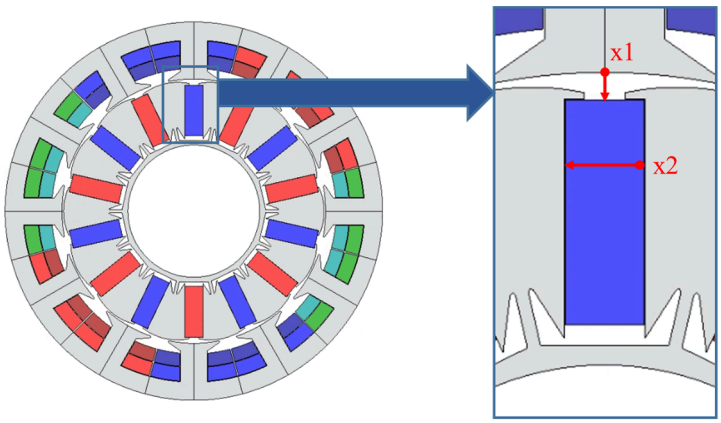


Figure 6. Selection of design variables.

The magnet width $x1$ determines the magnetic loading and directly affects the flux distribution in the rotor. A larger magnet width increases the magnetic flux but may also lead to higher magnet volume. The magnet stack length $x2$ influences the effective magnetic path and the demagnetization characteristics under fault conditions.

Since these parameters strongly affect both the demagnetization behavior and magnet usage, they are selected as the key design variables for the optimization process.

3.2. LHS (Step II)

In this step, sampling points are obtained to analyze the defined design variables. To achieve uniformly distributed combinations, LHS is performed. As shown in the result of Figure 7, 15 uniformly distributed sampling points are generated.

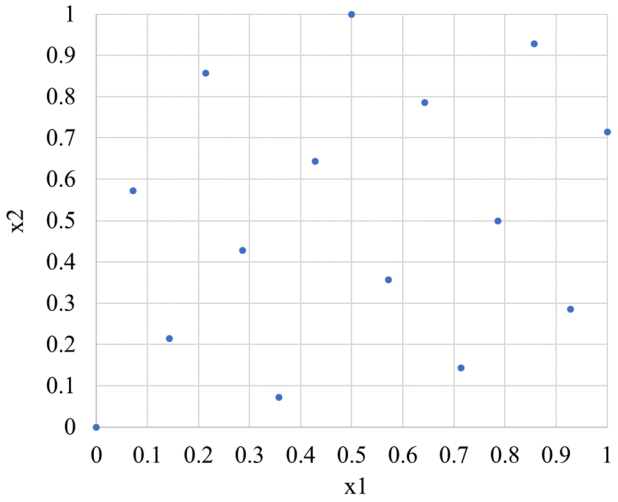


Figure 7. LHS-based sampling distribution of design variables.

3.3. FEM Analysis (Step III)

In the optimal design process of the quad-winding PMSM, the primary objective is to maintain 0% irreversible demagnetization under winding fault conditions while preserving the motor performance under healthy conditions.

To achieve this, FEM analysis was performed based on the selected design variables considering irreversible demagnetization and torque characteristics.

3.4. Function Approximation Using RBF–MLP Surrogate Model (Step IV)

In Step 4, a function approximation model is constructed by combining the RBF and the MLP based on the given input data, as shown in Figure 8. The input data are nonlinearly transformed by the RBF, and the transformed data are learned by the MLP. Through this process, the trained model can perform predictions for new input data.

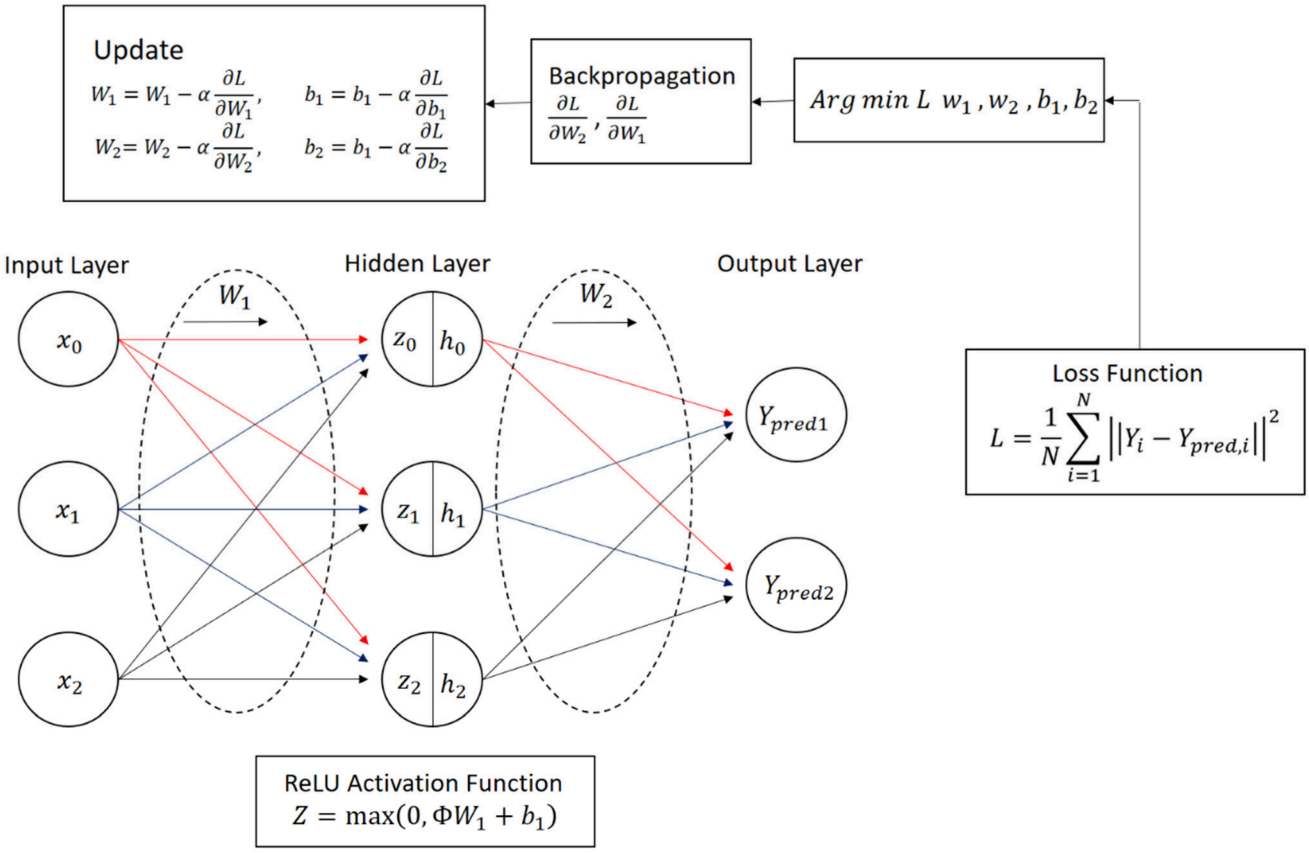


Figure 8. MLP model structure.

First, input and output data are defined. Input data consist of multiple samples, each having multiple features. The data are organized in a multidimensional matrix. The input–output relationship is then utilized to train the model. The input data are transformed using RBF, which applies a local response centered around a specific feature of the input data. This transformation function can be mathematically expressed as

$$\phi(x) = \exp\left(-\frac{||x - c||^2}{2\sigma^2}\right) \quad (1)$$

where x represents the input data, c is the center of the RBF, and σ is the hyperparameter that determines the width of the RBF. The transformed values construct a new fea-

ture space, which is then used as input for the MLP. The transformed input matrix Φ is defined as

$$\Phi_{ij} = \exp\left(-\frac{||X_i - C_j||^2}{2\sigma^2}\right) \quad (2)$$

The transformed feature matrix Φ is used as the input to a MLP to approximate the relationship between the design variables and the objective functions. The MLP consists of an input layer, hidden layers with nonlinear activation functions, and an output layer. In this study, the MLP is trained to predict the irreversible demagnetization ratio and magnet volume. The detailed formulations of the activation function, loss function, and backpropagation process are omitted for brevity, as they follow standard neural network methodologies [21–23]. After training, the surrogate model is used to evaluate the objective functions for new design variables, enabling efficient optimization without repeated FEM simulations.

3.5. Optimal Design of Quad-Winding PMSM (Step V)

The analysis results obtained at the LHS sample points are summarized in Table 2.

Table 2. Analysis Results at LHS Sample Points.

No.	x1	x2	y1	y2
1	2.4286	3.2143	2.3092	5.4
2	3.0714	3.0714	1.1286	5.3
3	3.7143	3.3571	0.4602	5.6
4	4.5714	3.9286	0.4233	6.1
5	4.7857	3.2857	0.3603	5.5
6	4.1429	3.1429	0.4476	5.4
7	2.2143	3.5714	2.1054	5.7
8	2.8571	3.4286	0.7497	5.6
9	3.9286	3.7857	0.4267	5.9
10	3.5000	4.0000	0.4638	6.1
11	3.2857	3.6429	0.4765	5.8
12	4.3571	3.5000	0.3471	5.7
13	2.0000	3.0000	5.9760	5.2
14	2.6429	3.8571	0.9062	6.0
15	5.0000	3.7143	0.3800	5.9

In this study, 15 LHS points were used considering the low-dimensional design space and computational cost of FEM analysis. The adequacy of the sampling points was evaluated based on the surrogate model prediction accuracy. A systematic convergence analysis to determine the optimal number of sampling points was not conducted and is left for future work. The results show that both the irreversible demagnetization ratio, y1, and the magnet volume, y2,vary with depending on the design variables $x1$ and $x2$.

The irreversible demagnetization ratio, y1, is defined as follows:

$$y_1 = \max\left(0, \frac{B_{initial} - B_{demag}}{B_{initial}} \times 100\right) \quad (3)$$

where $B_{initial}$ is the magnet flux density before demagnetization, and B_{demag} is the magnet flux density after irreversible demagnetization evaluation under the fault condition. The

demagnetization ratio is defined as a non-negative quantity. Negative values indicate that no irreversible demagnetization occurs and are therefore set to zero.

To visualize the relationship between the design variables and the objective functions, the response surfaces of $y1$ and $y2$ are illustrated in Figure 9. As shown in Figure 9a, the irreversible demagnetization ratio is minimized in a specific region of the design space. In contrast, Figure 9b shows that the magnet volume increases in the same region, indicating a trade-off relationship between the two objective functions.

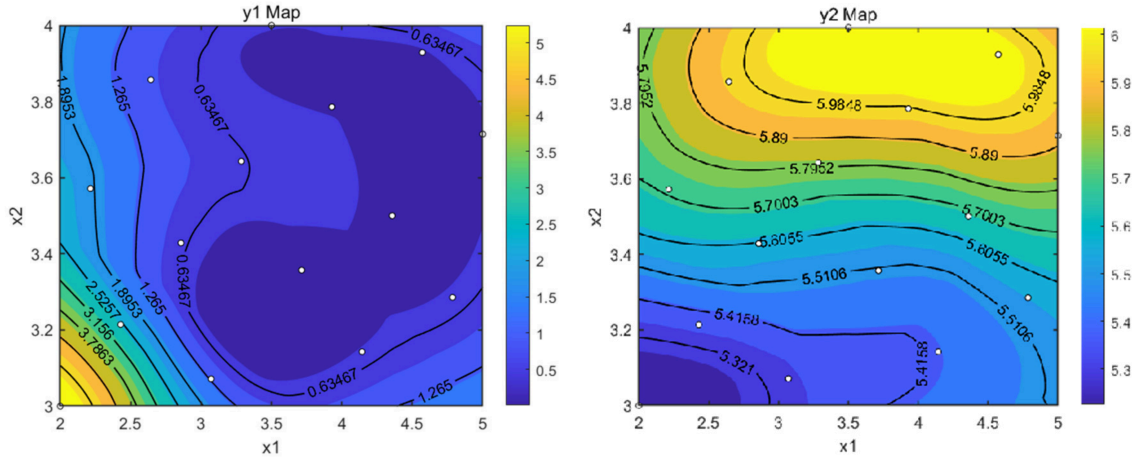


Figure 9. Surface plots of the objective functions: (**a**) Y1 (irreversible demagnetization ratio) and (**b**) Y2 (magnet volume).

Based on the response surface characteristics shown in Figure 9, the optimal design was obtained by applying the proposed optimization process. Figure 10 shows that irreversible demagnetization is effectively reduced in the optimized model. Table 3 summarizes the comparison between the initial design and the optimized design.

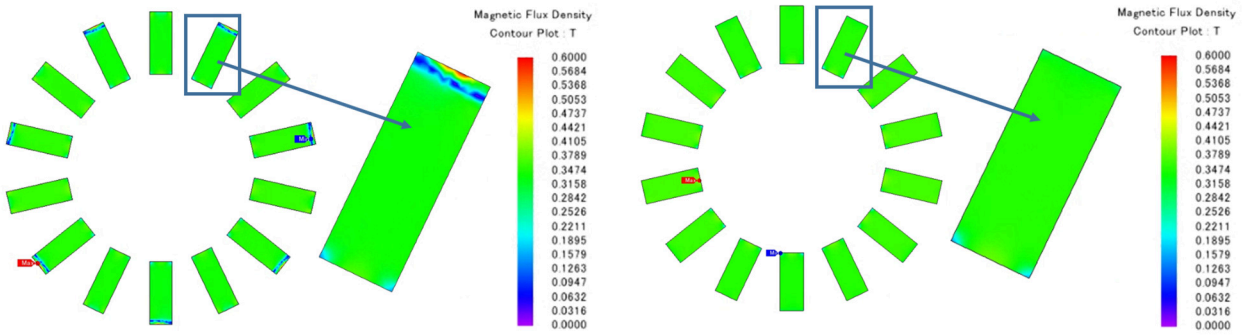


Figure 10. Irreversible demagnetization distribution in a spoke-type PMSM under three-winding fault conditions at maximum current: (**a**) initial model, (**b**) optimized model.

Table 3. Optimized Results.

Items		Unit	Initial Model	Optimized Model
Design variables	X1	mm	2	3.55
	X2	mm	3	3.17
Object functions	Y1 (Irreversible demagnetization ratio)	%	5.9	0.5
	Y2 (Magnet volume)	cm^3	5.2	5.4

The design variables X1 and X2 were adjusted from 2 mm and 3 mm to 3.55 mm and 3.17 mm, respectively. As a result, the irreversible demagnetization ratio Y1 was effectively reduced from 5.9% to 0.5%. Although the magnet volume Y2 slightly increased from 5.2 cm^3 to 5.4 cm^3, the optimized design effectively suppresses irreversible demagnetization while maintaining a similar magnet usage. These results confirm that the proposed optimization approach successfully reduces the irreversible demagnetization while keeping the magnet volume within a reasonable range.

4. Conclusions

This paper presents a fault-tolerant optimal design method for a quad-winding PMSM considering irreversible demagnetization. Under winding fault conditions, the external magnetomotive force acting on the permanent magnets increases due to current redistribution in the remaining windings, which can lead to irreversible demagnetization in spoke-type magnet structures. To address this issue, an optimization process based on an RBF–MLP model combined with grid-based search and local optimization is employed. The main contribution of this work is the establishment of a design process that explicitly accounts for the coupled relationship between fault-induced current redistribution and irreversible demagnetization in quad-winding PMSMs. A surrogate model is used to efficiently explore the design space and obtain a motor design that suppresses irreversible demagnetization while maintaining magnet volume. As a result, the optimized design reduces the irreversible demagnetization ratio from 5.9% to 0.5% with a similar magnet volume. However, this study is limited to electromagnetic analysis under predefined operating conditions and a specific pole pair configuration, and experimental validation is not included. Future work will focus on experimental validation and extension to more complex fault conditions and different pole pair designs.

Author Contributions: Conceptualization, M.-S.J. and K.-Y.H.; Methodology, M.-S.J., Y.-J.S. and K.-Y.H.; Software, Y.-J.S.; Validation, K.-i.W.; Formal analysis, Y.-J.S.; Data curation, K.-i.W.; Writing—original draft, M.-S.J. and K.-Y.H.; Writing—review and editing, Y.-J.S. and K.-Y.H.; Supervision, K.-i.W. and K.-Y.H.; Project administration, K.-i.W. All authors have read and agreed to the published version of the manuscript.

Funding: This work was supported by a Research Grant of Pukyong National University (2025).

Institutional Review Board Statement: Not applicable.

Informed Consent Statement: Not applicable.

Data Availability Statement: The original contributions presented in this study are included in the article. Further inquiries can be directed to the corresponding authors.

Conflicts of Interest: The authors declare no conflict of interest.

References

1. Zhu, Z.Q.; Howe, D. Electrical Machines and Drives for Electric, Hybrid, and Fuel Cell Vehicles. *Proc. IEEE* **2007**, *95*, 746–765. [CrossRef]
2. Wang, X.; Wang, Z.; He, M.; Zhou, Q.; Liu, X.; Meng, X. Fault-Tolerant Control of Dual Three-Phase PMSM Drives with Minimized Copper Loss. *IEEE Trans. Power Electron.* **2021**, *36*, 12938–12953. [CrossRef]
3. Yang, S.; Wang, M.; Wang, M.; Tong, C.; Zheng, P. Fault Reconstruction and Tolerance of Five-Phase Current-Source Drive System. *IEEE Trans. Ind. Electron.* **2025**, *72*, 14943–14948. [CrossRef]
4. Cheng, S.; Zhou, R.; Li, Z.; Zhao, J.; Xiang, C. Robust Model-Free Fault-Tolerant Predictive Control for PMSM Drive System. *IEEE Access* **2024**, *12*, 8502–8512. [CrossRef]
5. Huang, W.; Hua, W.; Chen, F.; Yin, F.; Qi, J. Model Predictive Current Control of Open-Circuit Fault-Tolerant Five-Phase Flux-Switching Permanent Magnet Motor Drives. *IEEE J. Emerg. Sel. Top. Power Electron.* **2018**, *6*, 1840–1849. [CrossRef]

6. Bianchi, N.; Bolognani, S.; Pre, M.D. Design of a Fault-Tolerant IPM Motor for Electric Power Steering. *IEEE Trans. Veh. Technol.* **2006**, *55*, 1102–1111. [CrossRef]
7. Muduli, U.R.; Beig, A.R.; Jaafari, K.A.; Alsawalhi, J.Y.; Behera, R.K. Interrupt-Free Operation of Dual-Motor Four-Wheel Drive Electric Vehicle Under Inverter Failure. *IEEE Trans. Transp. Electrif.* **2020**, *7*, 329–338. [CrossRef]
8. Li, H.Y.; Zhu, Z.Q.; Hua, H. Comparative Analysis of Flux Reversal Permanent Magnet Machines With Toroidal and Concentrated Windings. *IEEE Trans. Ind. Electron.* **2019**, *67*, 5278–5290. [CrossRef]
9. Barrero, F.; Duran, M.J. Recent Advances in the Design, Modeling, and Control of Multiphase Machines—Part I. *IEEE Trans. Ind. Electron.* **2015**, *63*, 449–458. [CrossRef]
10. Feng, T.; Hao, S.; Zhang, X.; Yang, T.; Wang, L. Development of a Fault-Tolerant Permanent-Magnet Synchronous Motor. *IEEE Access* **2019**, *7*, 146228–146239. [CrossRef]
11. Geng, Q.; Li, Z.; Wang, H.; Zhang, G.; Zhou, Z. Natural Fault-Tolerant Control with Minimum Copper Loss in Full Torque Operation Range for Dual Three-Phase PMSM Under Open-Circuit Fault. *IEEE Trans. Power Electron.* **2024**, *39*, 1279–1291. [CrossRef]
12. Kim, K.T.; Lee, Y.S.; Hur, J. Transient Analysis of Irreversible Demagnetization of Permanent-Magnet Brushless DC Motor with Interturn Fault Under the Operating State. *IEEE Trans. Ind. Appl.* **2014**, *50*, 3357–3364. [CrossRef]
13. Lee, B.H.; Jung, J.W.; Hong, J.P. An improved analysis method of irreversible demagnetization for a single-phase line-start permanent magnet motor. *IEEE Trans. Magn.* **2018**, *54*, 8206905. [CrossRef]
14. Yoon, K.Y.; Hwang, K.Y. Optimal Design of Spoke-Type IPM Motor Allowing Irreversible Demagnetization to Minimize PM Weight. *IEEE Access* **2021**, *9*, 65721–65729. [CrossRef]
15. Hwang, K.; Yang, B.; Rhyu, S.; Kim, B.; Kim, D.; Rhee, S.; Kwon, B. Optimal Rotor Design for Reducing the Partial Demagnetization Effect and Cogging Torque in Spoke-Type PM Motor. *J. Appl. Phys.* **2009**, *105*, 07F123. [CrossRef]
16. Hwang, K.Y.; Yoon, K.Y. Fault-Tolerant Design Process of Spoke-Type IPM Motor Considering Irreversible Demagnetization. *IEEE Trans. Magn.* **2022**, *58*, 8206809. [CrossRef]
17. Jeong, C.L.; Kim, Y.K.; Hur, J. Optimized Design of PMSM with Hybrid-Type Permanent Magnet for Improving Performance and Reliability. *IEEE Trans. Ind. Appl.* **2019**, *55*, 4692–4701. [CrossRef]
18. Yang, Y.J.; Kim, D.H.; You, Y.M. Demagnetization Analysis of Interior Permanent Magnet Synchronous Motors Under Realistic Vehicle Driving Conditions. *IEEE Access* **2026**, *14*, 123456–123467. [CrossRef]
19. Kim, K.T.; Lee, Y.S.; Hur, J. Analysis of Irreversible Demagnetization of Permanent Magnet Machines Considering Operating Conditions. *IEEE Trans. Ind. Appl.* **2020**, *56*, 3714–3723.
20. Hwang, K.Y.; Yoon, K.Y.; Song, B.K. System-Level Fault Tolerance Design Process of Dual-Winding Motors for Overheat in Integrated Electric Braking System of Autonomous Vehicle. *IEEE Trans. Veh. Technol.* **2022**, *72*, 3063–3073. [CrossRef]
21. Levi, E.; Bojoi, R.; Profumo, F.; Toliyat, H.A.; Williamson, S. Multiphase Induction Motor Drives—A Technology Status Review. *IEEE Trans. Ind. Electron.* **2007**, *1*, 489–516. [CrossRef]
22. Haykin, S. *Neural Networks and Learning Machines*, 3rd ed.; Prentice Hall: Upper Saddle River, NJ, USA, 2009.
23. Park, J.; Sandberg, I.W. Universal approximation using radial basis-function networks. *IEEE Trans. Neural Netw.* **1991**, *2*, 246–257. [CrossRef] [PubMed]

Disclaimer/Publisher's Note: The statements, opinions and data contained in all publications are solely those of the individual author(s) and contributor(s) and not of MDPI and/or the editor(s). MDPI and/or the editor(s) disclaim responsibility for any injury to people or property resulting from any ideas, methods, instructions or products referred to in the content.